HHS Public Access

Author manuscript

*Mol Cancer Ther*. Author manuscript; available in PMC 2017 August 01.

Published in final edited form as:

*Mol Cancer Ther*. 2016 August ; 15(8): 1809–1822. doi:10.1158/1535-7163.MCT-15-0688.

# Combination of eribulin and Aurora A inhibitor MLN8237 prevents metastatic colonization and induces cytotoxic autophagy in breast cancer

**Varvara K. Kozyreva**[1,*], **Anna A. Kiseleva**[2,9,*], **Ryan J. Ice**[1], **Brandon C. Jones**[2], **Yuriy V. Loskutov**[1], **Fatimah Matalkah**[1], **Matthew B. Smolkin**[3], **Kristina Marinak**[1], **Ryan H. Livengood**[3], **Mohamad A. Salkeni**[1,6], **Sijin Wen**[1], **Hannah W. Hazard**[1,4], **Ginger P. Layne**[1,5], **Callee M. Walsh**[10], **Pamela S. Cantrell**[10], **Greg W. Kilby**[10], **Sricharan Mahavadi**[8], **Neal Shah**[1], and **Elena N. Pugacheva**[1,2,#]

[1]West Virginia University Cancer Institute, West Virginia University School of Medicine, Morgantown, WV, USA 26506

[2]Department of Biochemistry, West Virginia University School of Medicine, Morgantown, WV, USA 26506

[3]Department of Pathology, West Virginia University School of Medicine, Morgantown, WV, USA 26506

[4]Department of Surgery, West Virginia University School of Medicine, Morgantown, WV, USA 26506

[5]Department of Radiology, West Virginia University School of Medicine, Morgantown, WV, USA 26506

[6]Department of Medicine, West Virginia University School of Medicine, Morgantown, WV, USA 26506

[7]Department of Biostatistics, West Virginia University School of Medicine, Morgantown, WV, USA 26506

[8]INBRE Program, West Virginia University School of Medicine, Morgantown, WV, USA 26506

[9]Department of Biochemistry and Biotechnology, Kazan Federal University, Kazan, Tatarstan, 420008

[10]Protea Biosciences, Inc. Morgantown, WV, USA 26505

## Abstract

[#]Corresponding author's information: Elena N. Pugacheva, Mailing address: Department of Biochemistry and West Virginia University Cancer Institute, PO Box 9142, 1 Medical Center Drive, West Virginia University School of Medicine, Morgantown, WV, 26506. Phone: (304) 293-5295; Fax: (304) 293-4667; epugacheva@hsc.wvu.edu.

[*]both authors (Kozyreva and Kiseleva) equally contributed to the completion of this work.

**Disclaimers:** This manuscript contains original work only and has not been published nor submitted elsewhere. All authors have directly participated in the planning, execution, and analysis of this study, and approved the submitted version of this manuscript.

**Conflicts of interest:** The authors declare no conflicts of interest.

Recent findings suggest that the inhibition of Aurora A (AURKA) kinase may offer a novel treatment strategy against metastatic cancers. In the current study, we determined the effects of AURKA inhibition by the small molecule inhibitor MLN8237 both as a monotherapy and in combination with the microtubule targeting drug eribulin on different stages of metastasis in triple negative breast cancer (TNBC) and defined the potential mechanism of its action. MLN8237 as a single agent and in combination with eribulin affected multiple steps in the metastatic process including migration, attachment, and proliferation in distant organs, resulting in suppression of metastatic colonization and recurrence of cancer. Eribulin application induces accumulation of active AURKA in TNBC cells providing foundation for the combination therapy. Mechanistically, AURKA inhibition induced cytotoxic autophagy via activation of the LC3B/p62 axis and inhibition of pAKT, leading to eradication of metastases, but has no effect on growth of mammary tumor. Combination of MLN8237 with eribulin leads to a synergistic increase in apoptosis in mammary tumors, as well as cytotoxic autophagy in metastases. This preclinical data provides a new understanding of the mechanisms by which MLN8237 mediates its anti-metastatic effects and advocates for its combination with eribulin in future clinical trials for metastatic breast cancer and early stage solid tumors.

### Keywords

AURKA; autophagy; adhesion; metastasis; PDX

## Introduction

Kinases are considered to be the first line targets for designing anti-cancer therapies, due to their suitability of inhibition and importance in cell signaling. Out of the three members of the Aurora Kinase family, Aurora Kinase A (AURKA) is well-known for its role in mitosis (1) and can be successfully targeted to inhibit proliferation (2). Elevated AURKA protein levels are a negative prognostic marker of breast cancer (BC) patient survival (3). BC cells have increased levels of active AURKA, which in turn could lead to an increase in mitotic slippage/escape and accumulation of aneuploid cells resulting in more aggressive cancer (4). The potent, highly selective and orally-available AURKA inhibitor MLN8237 (Alisertib, IC50=6.7 nmol/L) (5) is currently in Phase I–III clinical trials to treat solid and hematologic cancers (6). Treatment with AURKA inhibitors leads to multiple defects including mitotic deficiency, apoptosis (7), and senescence in multiple human tumor cell lines (6, 8). MLN8237 demonstrated promising antitumor activity towards hematologic, lymphatic and CNS malignancies (9–13). In Phase I–II trials for advanced solid tumors MLN8237 as single agent was able to stabilize the disease in few cases (14–17) (https://clinicaltrials.gov/). The antitumor activity of MLN8237 was also tested in combination with standard of care agents including paclitaxel (18). In some cases, combination therapy provided enhanced antitumor activity in comparison to either agent alone (19). Many metastatic BCs are resistant to taxanes and currently are treated with a non-taxane microtubule inhibitor, eribulin mesylate (20), which induces mitotic arrest and apoptosis (21, 22). Eribulin has been approved as a monotherapy for patients with metastatic BC (23). The therapeutic benefit of eribulin in combination treatment with AURKA inhibitors is currently unknown. The anti-tumor activity of AURKA inhibition towards BC cells *in vitro* has been reported (24–27).

Nevertheless, little is known about the effect of MLN8237 on metastasis as a process and the treatment of established metastases. We have previously reported on the inhibition of pulmonary metastases by AURKA inhibitors (28). The mechanisms behind this phenomenon are still unknown. In our current work, we analyzed step by step the effects of MLN8237 alone or in combination with eribulin to define the specific stages of metastasis most affected by the drugs. We also document their ability to eradicate distant metastases in mouse models of breast cancer and patient-derived xenografts via simultaneous inhibition of migration and proliferation, along with activation of cytotoxic autophagy. The combination of MLN8237 with eribulin results in increased apoptosis in mammary tumors leading to the additional benefit of local control and a drastic decrease in the number of bone metastases. Application of MLN8237 plus eribulin in adjuvant and metastatic settings could potentially lead to a significant regression of tumor growth in all sites, which would improve survival. In addition, observed activity in adjuvant settings may lead to a decrease in recurrence risk, thus improving disease-free survival and possibly overall survival in earlier stages.

## Materials and Methods

### Cell lines and reagents

BT-549 and MDA-MB-231LN cells were obtained in 2011–12 from ATCC and Caliper, amplified based on manufacturer's recommendations; multiple aliquots frozen, one aliquot of each was thawed for this project. All cell lines come with comprehensive authentication and quality assurance testing by ATCC/Caliper via Short Tandem Repeat profiling, no authentication was done by the authors. HCI_001, HCI_002 are TNBC primary cells kindly provided by Dr. Alana Welm (Huntsman Cancer Institute, University of Utah) through a shared MTA agreement; PEN65 ER+/PR+/HER2− primary cells from WVU Center Institute (West Virginia University) were freshly isolated in 2015 from patient-derived xenografts using previously published protocols (29), frozen and cultured less than one months, no authentication was done by the authors. All cells were routinely screened for the absence of mycoplasma. siRNAs, cell medium and supplements were prepared as previously described (28). Eribulin mesylate (Halaven™) was kindly provided by MBR Cancer Center pharmacy. MLN8237 and Chloroquine were purchased from SelleckChem and Sigma-Aldrich respectively.

### Cell proliferation and nuclear morphology analysis

Cell proliferation was determined using the CountessII Automated Cell Counter. $1x10^4$ cells were treated with serial dilutions: 0/25/50/100/150nM-MLN8237; 0/1/3/5nM-eribulin or combination in triplicates for 48h, n=3. Viable cells were counted based on trypan-blue exclusion assay. Nuclear morphology was analyzed in 100 cells/treatment, n=3 using Hoechst33342, cleaved-caspase-3 & Annexin-V (BD-Biosciences) staining under x100 objective, Axiovert200/Zeiss microscope. Annexin-V and cleaved-caspase-3 positive cells with condensed/fragmented DNA were counted as apoptotic. Cells with mitotic figures, large abnormally shaped nuclei, or multiple small nuclei were assigned in separate categories.

### Western blotting

Western blotting was performed using standard procedures (28). Primary antibodies included anti-AURKA (BD-Biosciences), -SQSTM1/p62, -LC3B, -Akt, -cleaved-PARP, -phospho-T288-AURKA (Cell Signaling), pAkt/S473 (R&D), -β-actin, -α-tubulin (Sigma), GAPDH (Millipore). Secondary anti-mouse, anti-rabbit HPR-conjugated antibodies (ImmunoResearch Labs), dilution 1:10,000 followed by chemiluminescence-based detection with HyGLO™ (DenvilleScientific). Bands were quantified using the digital electrophoresis documentation and image analysis software GeneTools (Syngene Corp.), with signal intensity normalized to β-actin/α-tubulin/or GAPDH.

### 3D-migration/invasion

Studies were carried out in 3D chemotaxis μ-slides (Ibidi) according to manufacturer's protocol. Briefly, attached cells were pretreated overnight with vehicle, 100nM-MLN8237, 3nM-eribulin or combination (100nM-MLN8237+3nM-eribulin); de-attached and $3x10^6$ cells/ml were suspended in 3mg/ml Matrigel (BD-Biosciences). Vehicle/or drugs were included in medium and Matrigel. Imaging was done using a Nikon-Sweptfield/Eclipse TE2000-E confocal microscope with 10X PlanApo DIC objective every 15 minutes for 23 hours. Time-lapse images were combined to build the video files and analyzed using ImageJ software/NIH. The tracks of individual cell movement were manually mapped using MTrackJ plug-in to measure cell body and leading edge speed, distance and directionality (30). Detailed analysis provided in Supplementary Methods.

### Immunofluorescent cell analysis

The cells were processed as previously described (31). Primary antibodies included anti-cleaved caspase-3, -LC3B, -SQSTM1/p62, phospho-mTOR/S2448, phospho-Bad/S112, phospho-Erk1/2 Thr202/Tyr204 (Cell Signaling), -pAkt/S473 (R&D), phospho-T288-AURKA (BethylLabs), -actin, α-tubulin (Santa Cruz), phospho-Histone H3 (BD-Biosciences). Secondary antibodies included AlexaFluor 488, 555, 647 (LifeTechnologies). Images were captured using the confocal microscope LSM-510/Zeiss equipped with Photometrics-QuantEM CCD camera (Photometrics), 63X Plan-Fluor, NA1.4 objective. Images were captured every 0.35μm, followed by 3D reconstruction using LSM/Zeiss and ImageJ/NIH software. The images inside each data set were collected with the same microscopy and image capture settings, and the raw data were used for image and statistical analysis.

### Fluorescence-activated cell sorting (FACS)

FACS was performed as previously described (32). The detailed protocol is provided in Supplementary Methods.

### Fluorescent immunohistochemistry (F-IHC)

The detailed F-IHC protocol and used antibodies are provided in Supplementary Material and Methods. IHC images were obtained using LSM-510/Zeiss fluorescent microscope, 20X objective. Images were analyzed and intensity was calculated via ImageJ software (NIH). For quantifications, the signal from corresponding antibodies was normalized by area and

number of nuclei. Metastases borders were determined by an overlay with H&E, nuclear morphology, cytokeratin staining, and interpreted by a pathologist.

### Anoikis assay

Attached cells were pre-treated with vehicle, 3nM-eribulin, 100nM-MLN8237 or combination for 24 hours, then trypsinized and placed on Ultra-Low attachment plates (Corning) with complete medium containing drugs as indicated above for 48 hours. Drugs were re-applied every 24 hours. Anoikis-induced apoptosis was detected via staining with Annexin-V-FITC (BD-Biosciences), propidium iodide (Sigma) containing 10ug/ml RNAse, or anti-cleaved-caspase-3 antibody (BD-Biosciences) via FACS.

### Cell adhesion and spreading assay

Cells were pretreated with drugs as above, trypsinized and $1\times10^4$ cells/well were plated in vehicle/or drugs-containing medium. Multiple bright-field images were taken at 10x magnification every 20 min for 1–2 hours. The area of individual attached cells were quantified using ImageJ software, 100 cells analyzed/per time point.

### Xenograft models of breast cancer and treatments

Orthotopic and tail vein injections were performed as previously described (28) approved Institutional Animal Care and Use Committee protocol. Treatment with vehicle, MLN8237/20mg/kg, eribulin/0.6mg/kg or combinations (MLN8237/10mg/kg, eribulin/0.3mg/kg) was initiated when primary tumors reached 500 $mm^3$, as measured by ultrasound Vevo2100 system (Visualsonics). In tail vein models mice were treated with similar regiments including chloroquine 20mg/kg and MLN8237 20mg/kg + chloroquine 20mg/kg. MLN8237 was administered via oral gavage twice daily for 4 days/week, 2–3 weeks (28). Eribulin was administrated every other day by intraperitoneal (IP) injection for 2–3 weeks. Chloroquine was administrated for 5 days/weeks by IP injected once daily for 2 weeks. At the end of the study the primary tumors, lungs, bones were collected and fixed. Consecutive 4–5μm sections were used for F-IHC and hematoxylin and eosin (H&E) staining followed by mitotic index quantification.

### Survival studies

Females: 500 $mm^3$ mammary tumors were resected, mice treated with vehicle/or MLN8237/20mg/kg for two weeks. Males: NSG mice were injected via tail vein with $1\times 10^5$ MDA-MB-231LN cells and treated one week post injection with a similar regiment. The last day of treatment was assigned as the starting point of survival study: “Day 0”. The mice were monitored daily for signs of weight loss and distress. Mice were euthanized when they reached critical health condition according to WVU/IACUC tumor guidelines.

### Patient Derived Xenograft (PDX) models

BC biopsies were collected through the WVU Cancer Institute or Cooperative Human Tissue Network (NCI) in accordance with WVU and CHTN-approved IRB protocol. 2x2$mm^3$ of tumor tissue was implanted into the pre-cleared $4^{th}$ inguinal mammary gland of NSG female mice for 2–6 months. 500$mm^3$ tumors (PDXs, Supplementary Table 1) were resected, mice

were treated as described above. Multiple internal organs were collected, fixed, and embedded in paraffin after treatment for pathological evaluation. Disseminated tumor cells in femurs were quantified from fresh bone marrow samples which were minced, plated in medium, and allowed to attach for 24 hours. For fixed samples, serial sections with 5μm intervals were made from each organ, stained with H&E, and analyzed for metastases.

### Time course study of metastatic colonization

Male NSG mice were injected with $1x10^5$-MDA-MB-231LN cells via tail vein injection. Immediately following injection of cancer cells, mice were treated with MLN8237/or vehicle as above. Mice were euthanized at 24, 48, and 72 hours post cell injection/initial treatment. Upon euthanasia, lungs were collected, fixed and embedded in paraffin. 5μm serial sections through the whole lungs were made, stained with H&E, and analyzed for metastases (single cell, clustered cells) by pathologist.

### Laser Ablation Electrospray Ionization Mass Spectrometry (LAESI-MS) analysis

Detailed protocol/analysis provided in Supplementary Methods.

### Statistical analysis

Statistical comparisons were made using two-tailed Student's t test. When more than two groups were analyzed, one-way or two-way analysis of variance (ANOVA) was used. $P \leq 0.05$ was considered to be significant (*) as indicated in figure legends. All treatment groups were compared to vehicle unless mentioned otherwise. Experimental values were reported as the means with +/-S.E.M (standard error of mean) and calculations of statistical significance were made using GraphPad software. Additional statistical methods including synergy analysis are provided in Supplementary Methods.

## Results

### Application of eribulin leads to an increase in active AURKA

In our study we found that application of FDA approved BC anti-metastatic agent eribulin as a single agent results in a significant increase in the active form of AURKA in TNBC cells and xenografts (Fig. 1A–B, Fig. S1A–B). The combination of eribulin with MLN8237 eliminates this effect and decreases amount of active AURKA. To test if AURKA expression could be a potential biomarker of the patient's response to eribulin, we depleted AURKA via application of anti-AURKA siRNAs and assessed the viability of cells. The decrease in AURKA expression resulted in little to no effect on viability of MDA-MB-231 cells, which have mutant p53 and significant upregulation of endogenous AURKA. Depletion of AURKA in the patient-derived TNBC cell line HCI_002 potentiated eribulin treatment and resulted in an increase in cell death (Fig. S1C–D), suggesting that combination of these drugs might significantly improve the treatment outcomes of metastatic BC patients. Next, we tested the effects of MLN8237 and combination on different stages of metastatic cascade.

### MLN8237 and eribulin reduce 3D motility/invasion and adhesion of BC cells

We have previously reported that the activity of AURKA is critical for stabilization of actin at the leading edge of migrating tumor cells (31). Cells treated with eribulin also show decreased motility (22). In the current work, we have tested the impact of AURKA inhibition as a single agent or in combination with eribulin on 3D migration/invasion using time-lapse microscopy. The treatment of TNBC cells embedded in basal membrane-like matrix (Matrigel) with MLN8237 reduces the speed, distance, and directionality of cell movement (Fig. 1C–E; Fig. S1E–H; Suppl.video 1–2). Interestingly, eribulin alone decreased directionality, but not the speed of cell migration, suggesting a different mode of action. Importantly, the combination of drugs resulted in a greater decrease in cell invasion and thus may significantly decrease the initial dissemination of tumor cells from the primary site.

Adhesion is an important step in cancer cells intra/extravasation to colonize distant organs. We tested if MLN8237 alone or in combination with eribulin impairs the ability of BC cells to attach to a physiologically relevant matrix. There was a significant decrease in the ability of cancer cells to attach/spread upon treatment with MLN8237 (Fig. 1F–G), suggesting that AURKA activity is required for formation/stabilization of cell/matrix adhesions, but the combination with eribulin did not result in an additional benefit.

### MLN8237, eribulin, or combination does not affect sensitivity of BC cells to anoikis

Circulating tumor cells (CTCs) released by solid tumors must develop a resistance to anoikis and survive in the blood/lymphatic system in order to reach distant organs. To test if inhibition of AURKA or application of eribulin may sensitize BC cells to anoikis, attached cells were pre-treated with drugs or vehicle for 24h, de-attached and re-plated on low attachment plates for 48h in the presence of drugs or vehicle. Fluorescence-activated cell sorting (FACS) and microscopy-based observation of nuclear morphology documented no difference in sensitivity to anoikis between the treatment groups based on Annexin-V, cleaved caspase-3, or propidium iodide staining (Fig. 2A–C), suggesting that neither MLN8237 nor eribulin have any effect on anoikis sensitivity in TNBC cells.

### Combination of eribulin and MLN8237 leads to synergistic induction of cell death in attached BC cells

Treatment of BC cells attached to the matrix with MLN8237 or eribulin has little to moderate effect on the induction of cell death with 5–10% of cells found to be Annexin-V, cleaved PARP, or PI positive 48h post treatment. Importantly, combination of these drugs led to a synergistic increase in the number of dead cells (Fig. 2D–E, FACS charts: Fig. S2). Attached BC cells were further tested for sensitivity to combination therapy via serial dilutions of both drugs (Fig. 2F). The number of live/dead cells after 48h of treatment in each dilution was used for assessment of drug interaction *in vitro* using three different statistical methods as described in the Supplementary Methods. The statistical analysis confirmed a synergistic mode of interaction between these drugs (Table 1).

### MLN8237 alone or in combination reduces metastases *in vivo* through the inhibition of proliferation/pro-survival pathways and promotion of cytotoxic autophagy

To determine the impact of MLN8237 and eribulin therapy on mammary tumors and established metastases, we utilized BC orthotopic xenograft models. MDA-MB-231LN, cells were injected in the mammary fat pad of NSG mice to form a mammary tumors ($500mm^3$) then treated with drugs as indicated. In agreement with our previous findings, MLN8237 did not suppress the growth of mammary tumors, however it drastically reduced the number of pulmonary metastases (Fig. 3A–B,E) (28, 31). The combination therapy led to significant reduction in the size of mammary tumor and metastases (Fig. 3B). Interestingly, eribulin alone has no effect on the number of metastases, but reduces their size when compared to vehicle (Fig. 3A), suggesting cytostatic rather than cytotoxic activity in lungs.

To define the potential mechanisms, we analyzed lung metastases and mammary tumors for expression of markers for proliferation (Ki67, pERK1/2), survival (pAKT/S473, p-mTOR/S2448), apoptosis (cleaved caspase-3, pBAD/S112), and autophagy (LC3B, p62/SQSTM1) via quantitative fluorescent IHC staining and western blot analysis. MLN8237, eribulin, and combination treatments decrease the proliferation and survival of tumor cells at the metastatic site (lungs) by 80–90%, as indicated by decreases in Ki67 expression and phosphorylation of AKT (Fig. 3C, E) and its downstream substrates mTOR (33) and BAD (34) (Fig. S3A–B). The activity of caspase-3, a prominent marker of apoptosis, was not affected in metastases while slight decrease in phosphorylation of BAD a proapoptotic member of the Bcl-2 family indicates autophagy-promoting effect of BAD, potentially via release of Beclin1 from Bcl2 complex (35). Expression of p62/SQSTM1 and LC3B significantly increased, in MLN8237 and combination-treated metastases, but not in metastases treated with eribulin alone, suggesting the involvement of autophagy in the clearance of metastases (Fig. 4A, C).

The effect of MLN8237 on proliferation/Ki67 of mammary tumor cells was lower, but statistically significant, with minimal changes in pAKT and p-mTOR (Fig. 3D, F; Fig. S3C–D,F). The increase in pERK1/2 and pBAD which might be indicative of active cell cycle and inhibition of apoptosis (36) was significant in MLN8237-treated tumors (Fig. S3C–D). MLN8237 treatment did not induce upregulation of p62/LC3B or activation of caspase-3 in mammary tumors in agreement with the limited effect on tumor size.

Eribulin and combination therapy, however, significantly reduced the size of mammary tumors, which correlates with the decrease in Ki67, p-mTOR, pERK1/2, pBAD and increase in p62, LC3B, and cleaved caspase-3 expression (Fig. 4B, D; Fig. S3C–D), which suggests involvement of both pathways (autophagy and apoptosis) in the reduction of mammary tumors. pAKT was slightly upregulated in eribulin and combination-treated mammary tumors, which correlates with the re-distribution of AKT from the nucleus (observed in vehicle and MLN8237) to the cytoplasm, which was previously shown to correlate with induction of apoptosis (37). The DNA panels for the IHC staining are included in Fig. S4. In addition to H&E staining and nuclear morphology, metastases were confirmed via cytokeratin staining (Fig. S5).

Next, we analyzed the lysates prepared from mammary tumors and lung metastases using western blotting to assess the levels of the indicated above markers. MLN8237 increased LC3B staining and conversion to the LC3B-II form in lysates of lung metastases, but not in mammary tumors (Fig. S6A–C). Due to the small size of the eribulin and combination-treated mammary tumors and lung metastases, the levels of cleaved caspase-3, p62 and pAKT were not detectable.

As a complementary approach, we amplified and treated *in vitro* the tumor cells isolated from mammary tumors and lungs of vehicle-treated mice. Expression of most markers was similar to the levels observed in tumors and metastases by IHC, but the levels of p62 and pAKT did vary and were on average higher in mammary tumor cells than lung metastases (Fig. 4E). Cleaved PARP, a downstream target of active caspase-3, was elevated in eribulin and combination-treated cells, suggesting an activation of apoptosis, which is in agreement with the IHC data. Addition of chloroquine, an inhibitor of autophagy, resulted in further increases in p62 and LC3B in cells isolated from both sites, suggesting that *in vitro*, both types of cells had significant levels of basal autophagy potentially due to *in vitro* culturing conditions (Fig. 4E–F).

Similar to F-IHC data, immunofluorescent staining of p62 in MLN8237-treated cells isolated from lung metastases shows upregulation of p62 and decrease in pAKT. Addition of chloroquine leads to further increase in p62 levels indicating the presence of active autophagic flux (Fig. S7A–B). Immunofluorescent staining of p62 in cells isolated from MLN8237-treated mammary tumors shows active autophagic flux only in eribulin and combination-treated cells (Fig. S7C–D). Analysis of nuclear morphology in these cells shows a significant increase in apoptotic and polynucleated cells upon treatment with eribulin or combination, while MLN8237 causes an increase in abnormally shaped nuclei, potentially due to an increase in aneuploidy (Fig. S7E–F).

## MLN8237 reduces colonization potential of metastatic cells

Since only MLN8237 or combination therapy was able to decrease the number and size of pulmonary metastases, the effect of MLN8237 as a single agent on seeding and colonization of new metastases by circulating tumor cells was tested. MDA-MB-231LN cells were injected intravenously into NSG male mice via tail vein and immediately treated with vehicle or MLN8237 (Fig. 5A). The total flux and average radiance of injected animals was measured, but did not significantly differ during the experimental time frame. Mice were euthanized and lungs were harvested at 24, 48 and 72 hours post injection/treatment. Note that based on our previously published work and *in vitro* results, treatment with MLN8237 did not affect the viability of tumor cells in suspension (28). In agreement with these findings, a similar number of single-cell metastases was found in the lungs of mice at 24 hours post-injection. By 48 hours, in both MLN8237 and vehicle treated groups, some of the single-cell foci underwent one to two rounds of division forming “mixed metastases”, represented by a combination of single-cell and 2–4 cells clusters (Fig. 5B–C). However, by 72 hours of treatment, MLN8237 was able to reduce both the size and also total number of metastases (independent of size) in lungs (Fig. 5D). Under these conditions, the potential

difference in the number of cells in circulation released by primary tumors was eliminated, suggesting that MLN8237 specifically inhibits the colonization and growth of metastases.

## MLN8237 treatment improves overall survival via eradication of metastases by cytotoxic autophagy

To assess the impact of MLN8237 on overall survival, we injected BC cells into the mammary fat pad, followed by mammary tumor growth ($500mm^3$) and surgical resection. Mice were then treated with MLN8237 or vehicle in adjuvant settings for two weeks (Fig. 5E). After treatment, mice were monitored daily and then euthanized once a critical health condition was reached based on a veterinarian evaluation. Importantly, MLN8237 treatment in an adjuvant setting was able to increase the lifespan of mice by 31%, increasing from an average survival age of 19 days post-treatment in the control group to 32 days in the MLN8237-treated group. Twelve percent of MLN8237-treated mice remained tumor free until they were euthanized at 2 years old after the end of the study (Fig. 5F), indicating that MLN8237 significantly prolongs survival when used as a post-operative standard of care treatment. Interestingly, only half of the MLN treated animals had a recurrent mammary gland tumor when compared to the control group (Fig. 5G). In order to assess the impact of MLN8237 on the survival of animals with metastases in a gender unbiased assay and independent from possible mammary tumor size differences or surgery quality, BC cells were introduced via tail vein injection into male mice (Fig. 5H). Treatment with MLN8237 prolonged the survival of males twice more efficiently (by 62%) in the tail vein model, going from a median survival of 28 days in the control group to 46 days in the MLN8237-treated group (Fig. 5I–J). Similar to our earlier findings, the decrease in proliferation and survival markers was observed in lung metastases upon MLN8237 treatment (Fig. S8A–B). To determine that decrease in metastases is driven by cytotoxic autophagy we have performed similar metastatic colonization/growth study with addition of chloroquine – inhibitor of autophagy. Chloroquine alone did not affect metastatic growth when compared to vehicle but its addition to MLN8237 completely blocked MLN's potential to suppress metastatic outgrowth confirming pivotal role of autophagy in eradication of metastases *in vivo* (Fig. 5K–M).

## MLN8237 is efficient against pulmonary metastases in PDX models

To further evaluate our findings in clinically relevant models, we utilized metastatic breast cancer patient derived xenografts (PDXs). PDX models are significantly better at predicting drug responses in clinic and can replicate the heterogeneity of an original tumor (38). Five metastatic PDXs (Supplementary Table 1) were used in this study: HCI_001, HCI_002, PEN27, PEN25 and PEN65. Passage one PDXs (first transplantation after successful graft of patient's tumor biopsy, Fig. 5N–O) were used for drug evaluation. The grafted tumors ($500mm^3$) were surgically removed and mice were treated with MLN8237/or vehicle for two weeks; internal organs and mammary tumors (if re-grown) were collected for pathological evaluation. PDX-produced metastases were found in the lungs, lymph nodes, bones and brain. Number of metastases was significantly lower in the MLN8237-treated group (Fig. 5O). Recurrence rates of PDX mammary tumors were also significantly decreased upon treatment with MLN8237, suggesting that AURKA targeting may be critical for eradication of the cancer stem-like cells that are responsible for cancer relapse.

### MLN8237 plus eribulin is efficient strategy to control local and distant tumor growth

To gain local control and reduce the number of tumor cells disseminating from the primary site, the combination of MLN8237 with eribulin was tested. First, we tested the effect of combination therapy on growth/viability of primary tumor cells isolated from PDXs (HCI_002 and PEN65). Combination therapy led to significant decrease in proliferation and viability of cells (Fig. 6A–B, Fig. S9A–B) when compared to either drug alone. In the case of PEN65, a synergistic decrease in proliferation and increase in apoptosis was observed in combination (Table 2). Nucleus morphology analysis of the of HCI_002 and PEN65 cells treated with combination of eribulin and MLN8237 showed an increase in the number of cells with condensed/fragmented (apoptotic) DNA and polynucleated or abnormally shaped nuclei, and a decrease in a number of mitotic cells (Fig. 6B, Fig. S9B). Similar to MDA-MB-231LN, the patient-derived cells demonstrated an increase in cleaved caspase-3 staining (Fig. 6C–D). Cells treated with combination therapy also had increased levels of p62 (Fig. 6E). To assess the impact of combination therapy on PDX-mammary tumor growth *in vivo*, HCI_002 tumor fragments were transplanted into mammary fat pads of naïve NSG mice, and established tumors ($500mm^3$) were treated with vehicle/or drugs for 3 weeks. The combination therapy led to a 70–80% reduction in volume of PDX-mammary tumors versus 40% with eribulin alone (Fig. 6F, week 2). Statistical analysis using a mixed model shows the significant benefit of combination even with twice less dosage of each drug, suggesting a superior performance with an increase in dosage (Fig. 6G). The mitotic index in mammary tumors was decreased in animals treated with eribulin and combination, but not with MLN8237 alone, while in lung metastases only MLN8237 and combination treatment had a significant decrease in mitotic index (Fig. 6H). Additionally, the number of disseminated tumor cells to the bone was significantly decreased in eribulin and combination-treated animals, potentially due to the overall decrease in tumor volume or specific action of eribulin on dormant cancer cells in this microenvironment (Fig. 6I). Notably, eribulin had no effect on the number of disseminated tumor cells to the lungs (Fig. 6J).

To test if the limited MLN8237 efficacy in the mammary tumor is a result of poor penetration of the drug, we performed a drug distribution analysis in PDX tumors resected from mice treated with MLN8237 for 2 days using LAESI mass spectrometry imaging (Protea Biosciences). We demonstrate that based on histological morphology, MLN8237 is present in and around the blood vessels of the tumor (Fig. S10A–C). Localization was further confirmed by a correlative high content of heme-groups (Fig. S10D–F).

## Discussion

This study identifies the specific stages of the metastatic process that are most efficiently inhibited by the investigational compound MLN8237 (Alisertib), both as a single agent and in combination with the FDA approved drug eribulin mesylate (Halaven) to benefit metastatic BC patient care. The application of eribulin leads to significant accumulation of cells with active AURKA justifying the introduction of combination therapy to clinic. AURKA is known to be a pro-migratory and pro-invasive kinase (26, 31). Our findings indicate that MLN8237 alone or in combination with eribulin reduces the adhesion, speed and directionality of individual cell invasion, but did not affect the sensitivity of TNBC cells

to anoikis using *in vitro* and *in vivo* models. Promising results of the anti-proliferative effect of MLN8237 were previously shown in breast cancer orthotopic models (39) if applied at early stages. Our previous studies in TNBC cell lines MDA-MB-231 and BT-549, however, showed resistance of established mammary tumors to MLN8237 treatment (28, 31). The effects of MLN8237+eribulin combination on cancer cells in the metastatic niche are currently unknown.

Our study shows that MLN8237 alone or in combination with eribulin reduces proliferation of BC cells in lung metastases, suggesting a specific effect of MLN8237 on metastatic cells. Eribulin and combination therapy both reduced proliferation of the primary tumor. MLN8237 treatment also decreased the survival of cancer cells *in vitro and in vivo* (39) via a reduction in phosphorylation of AKT in metastases, but not primary tumors. Phosphorylated AKT was mainly found in the nucleus of tumors treated with vehicle and MLN8237, and was found to be cytoplasmic in eribulin and combination-treated tumors, suggesting the activation of apoptosis in the latter cases. The treatment of tumor cells in culture did not result in significant changes in AKT or its translocation to the nucleus, suggesting that *in vitro* conditions have some limitations to reproduce the *in vivo* phenotype.

The impact of AURKA inhibition on apoptosis is controversial so far, with some reports suggesting that AURKA inhibition induces apoptosis (9, 40, 41) and other reports considering the impact of AURKA inhibition on apoptosis to be insignificant (27). The effect of MLN8237 on BC cell apoptosis in metastases was not documented. In our study, inhibition of AURKA did not induce caspase-3-dependent apoptosis in pulmonary metastases or the mammary tumor. It is possible that there is an apoptotic effect of MLN8237 which is not caspase-3-dependent. However, our results indicate that MLN8237 treatment induces cytotoxic autophagy specifically in pulmonary metastases, which may significantly contribute to the anti-metastatic effect of MLN8237. It has been shown that autophagy can cause cancer cell death in a caspase-3-independent manner (42, 43). An increase in autophagy can also facilitate cancer survival (cytoprotective autophagy) and has been documented in some tumors treated with anti-cancer drugs (44). While it still might be the case in the primary mammary tumor, MLN8237 clearly induces cytotoxic autophagy in metastases, as indicated by a decrease in pAKT and an increase in p62 and processed form of LC3B. Eribulin alone or in combination induces apoptosis in TNBC cells based on the presence of cleaved PARP and caspase-3, but simultaneously increases the level of autophagy markers p62 and LC3B. It was previously shown that apoptosis can suppress autophagy, and thus, accumulation of p62 and LC3B may reflect the inhibition of autophagic flux. To test for this possibility, we co-treated cells with autophagy inhibitor chloroquine along with MLN8237/or eribulin. Chloroquine treatment led to further increase in p62 and LC3B, which argues against the inhibition of autophagic flux and supports the idea of potential cooperation between both types of cell death in combination therapy. The combination therapy provided synergistic activation of apoptosis, leading to an increase in cell death, drastically reducing tumor mass at the primary site and metastases in multiple sites, including bone lesions, which are the most common and difficult to treat. Even at the half dosages used in combination, the effect was superior to either drugs with twice higher concentration, suggesting that usage of this regiment may significantly reduce side effects of therapy in the clinic.

The mass spectrometry analysis of flash frozen mammary tumors isolated from MLN8237 treated animals is indicative of blood-based MLN8237 delivery/distribution in the tumor tissue. Thus, tumors with limited blood vessel density may experience limited effects of MLN8237 when compared to lung lesions. In agreement with our findings, limited pre-clinical and clinical efficacy of MLN8237 was documented in the treatment of solid tumors, where MLN8237 could stabilize the disease, but was incapable of reducing the tumor size (15), meanwhile, blood malignancies in xenograft mouse models show an extreme sensitivity to the MLN8237 compound (11). In both a xenograft model which incorporates the influence of primary tumor invasion and extravasation, and tail-vein injection model, which takes into account only the metastatic colonization stage of disease, we showed that the treatment with MLN8237 significantly increases survival rates. It is expected that combination treatment will improve survival to an even greater degree than MLN8237 alone. Previously, MLN8237 was shown to increase survival in neuroblastoma (45) and acute myelogenous leukemia models (9). Here we present the first evidence of such an effect on metastatic BC using patient derived xenografts (PDXs). The recent findings presented at the 2014 San Antonio Breast Cancer Symposium show that breast cancer PDX models most accurately predicted the patient clinical response. Importantly, when combined with eribulin, MLN8237 demonstrates synergistic inhibition of primary tumor and metastases growth, including seeding of the metastases. Our findings indicate that MLN8237 plus eribulin can be used in adjuvant and metastatic settings to improve disease-free survival for BC patients.

## Supplementary Material

Refer to Web version on PubMed Central for supplementary material.

## Acknowledgments

**Financial Support**: This work was supported by grants from the NIH/NCI, CA148671 awarded to E.N. Pugacheva; IDeA CTR NIH/NIGMS, U54GM104942 pilot award to E.N. Pugacheva, and in part by a NIH/NCRR 5 P20 RR016440-09 award to MBR Cancer Center. S. Mahavadi was supported by the WV-INBRE grant 5P20GM103434-13. A.A. Kiseleva was partially supported by the funds from program of competitive growth of Kazan Federal University. The Animal Models & Imaging, Microscope Imaging and WVU Flow Cytometry Core Facilities were supported by the MBRCC and the NIH grants P20-RR016440, GM103488/RR032138, S10RR026378, S10-RR020866, S10-OD016165, and GM103434. Some of the tissue samples for PDXs were provided by the Cooperative Human Tissue Network, which is funded by the National Cancer Institute.

We thank the HSC Core Facilities, WVU Cancer Institute and Biochemistry Department for their outstanding administrative support.

## References

1. Glover DM. Aurora A on the mitotic spindle is activated by the way it holds its partner. Mol Cell. 2003; 12:797–9. [PubMed: 14580330]
2. Gadea BB, Ruderman JV. Aurora kinase inhibitor ZM447439 blocks chromosome-induced spindle assembly, the completion of chromosome condensation, and the establishment of the spindle integrity checkpoint in Xenopus egg extracts. Mol Biol Cell. 2005; 16:1305–18. [PubMed: 15616188]
3. Nadler Y, Camp RL, Schwartz C, Rimm DL, Kluger HM, Kluger Y. Expression of Aurora A (but not Aurora B) is predictive of survival in breast cancer. Clin Cancer Res. 2008; 14:4455–62. [PubMed: 18628459]

4. Liu Q, Ruderman JV. Aurora A, mitotic entry, and spindle bipolarity. Proc Natl Acad Sci U S A. 2006; 103:5811–6. [PubMed: 16581905]
5. Agnese V, Bazan V, Fiorentino FP, Fanale D, Badalamenti G, Colucci G, et al. The role of Aurora-A inhibitors in cancer therapy. Ann Oncol. 2007; 18(Suppl 6):vi47–52. [PubMed: 17591831]
6. Manfredi MG, Ecsedy JA, Meetze KA, Balani SK, Burenkova O, Chen W, et al. Antitumor activity of MLN8054, an orally active small-molecule inhibitor of Aurora A kinase. Proc Natl Acad Sci U S A. 2007; 104:4106–11. [PubMed: 17360485]
7. Hoar K, Chakravarty A, Rabino C, Wysong D, Bowman D, Roy N, et al. MLN8054, a small-molecule inhibitor of Aurora A, causes spindle pole and chromosome congression defects leading to aneuploidy. Mol Cell Biol. 2007; 27:4513–25. [PubMed: 17438137]
8. Huck JJ, Zhang M, McDonald A, Bowman D, Hoar KM, Stringer B, et al. MLN8054, an inhibitor of Aurora A kinase, induces senescence in human tumor cells both in vitro and in vivo. Mol Cancer Res. 2010; 8:373–84. [PubMed: 20197380]
9. Gorgun G, Calabrese E, Hideshima T, Ecsedy J, Perrone G, Mani M, et al. A novel Aurora-A kinase inhibitor MLN8237 induces cytotoxicity and cell-cycle arrest in multiple myeloma. Blood. 2010; 115:5202–13. [PubMed: 20382844]
10. Kelly KR, Nawrocki ST, Espitia CM, Zhang M, Yang JJ, Padmanabhan S, et al. Targeting Aurora A kinase activity with the investigational agent alisertib increases the efficacy of cytarabine through a FOXO-dependent mechanism. Int J Cancer. 2012; 131:2693–703. [PubMed: 22488249]
11. Manfredi MG, Ecsedy JA, Chakravarty A, Silverman L, Zhang M, Hoar KM, et al. Characterization of Alisertib (MLN8237), an investigational small-molecule inhibitor of aurora A kinase using novel in vivo pharmacodynamic assays. Clin Cancer Res. 2011; 17:7614–24. [PubMed: 22016509]
12. Mahadevan D, Stejskal A, Cooke LS, Manziello A, Morales C, Persky DO, et al. Aurora A inhibitor (MLN8237) plus vincristine plus rituximab is synthetic lethal and a potential curative therapy in aggressive B-cell non-Hodgkin lymphoma. Clin Cancer Res. 2012; 18:2210–9. [PubMed: 22374334]
13. Hong X, O'Donnell JP, Salazar CR, Van Brocklyn JR, Barnett KD, Pearl DK, et al. The selective Aurora-A kinase inhibitor MLN8237 (alisertib) potently inhibits proliferation of glioblastoma neurosphere tumor stem-like cells and potentiates the effects of temozolomide and ionizing radiation. Cancer Chemother Pharmacol. 2014; 73:983–90. [PubMed: 24627220]
14. Cervantes A, Elez E, Roda D, Ecsedy J, Macarulla T, Venkatakrishnan K, et al. Phase I pharmacokinetic/pharmacodynamic study of MLN8237, an investigational, oral, selective aurora a kinase inhibitor, in patients with advanced solid tumors. Clin Cancer Res. 2012; 18:4764–74. [PubMed: 22753585]
15. Dees EC, Cohen RB, von Mehren M, Stinchcombe TE, Liu H, Venkatakrishnan K, et al. Phase I study of aurora A kinase inhibitor MLN8237 in advanced solid tumors: safety, pharmacokinetics, pharmacodynamics, and bioavailability of two oral formulations. Clin Cancer Res. 2012; 18:4775–84. [PubMed: 22767670]
16. Macarulla T, Cervantes A, Elez E, Rodriguez-Braun E, Baselga J, Rosello S, et al. Phase I study of the selective Aurora A kinase inhibitor MLN8054 in patients with advanced solid tumors: safety, pharmacokinetics, and pharmacodynamics. Mol Cancer Ther. 2010; 9:2844–52. [PubMed: 20724522]
17. Kelly KR, Shea TC, Goy A, Berdeja JG, Reeder CB, McDonagh KT, et al. Phase I study of MLN8237--investigational Aurora A kinase inhibitor--in relapsed/refractory multiple myeloma, non-Hodgkin lymphoma and chronic lymphocytic leukemia. Invest New Drugs. 2014; 32:489–99. [PubMed: 24352795]
18. Scharer CD, Laycock N, Osunkoya AO, Logani S, McDonald JF, Benigno BB, et al. Aurora kinase inhibitors synergize with paclitaxel to induce apoptosis in ovarian cancer cells. J Transl Med. 2008; 6:79. [PubMed: 19077237]
19. Anand S, Penrhyn-Lowe S, Venkitaraman AR. AURORA-A amplification overrides the mitotic spindle assembly checkpoint, inducing resistance to Taxol. Cancer Cell. 2003; 3:51–62. [PubMed: 12559175]

20. Dabydeen DA, Burnett JC, Bai R, Verdier-Pinard P, Hickford SJ, Pettit GR, et al. Comparison of the activities of the truncated halichondrin B analog NSC 707389 (E7389) with those of the parent compound and a proposed binding site on tubulin. Mol Pharmacol. 2006; 70:1866–75. [PubMed: 16940412]
21. Kuznetsov G, Towle MJ, Cheng H, Kawamura T, TenDyke K, Liu D, et al. Induction of morphological and biochemical apoptosis following prolonged mitotic blockage by halichondrin B macrocyclic ketone analog E7389. Cancer Res. 2004; 64:5760–6. [PubMed: 15313917]
22. O'Rourke B, Yang CP, Sharp D, Horwitz SB. Eribulin disrupts EB1-microtubule plus-tip complex formation. Cell Cycle. 2014; 13:3218–21. [PubMed: 25485501]
23. Cortes J, O'Shaughnessy J, Loesch D, Blum JL, Vahdat LT, Petrakova K, et al. Eribulin monotherapy versus treatment of physician's choice in patients with metastatic breast cancer (EMBRACE): a phase 3 open-label randomised study. Lancet. 2011; 377:914–23. [PubMed: 21376385]
24. Wang LH, Xiang J, Yan M, Zhang Y, Zhao Y, Yue CF, et al. The mitotic kinase Aurora-A induces mammary cell migration and breast cancer metastasis by activating the Cofilin-F-actin pathway. Cancer Res. 2010; 70:9118–28. [PubMed: 21045147]
25. Wang F, Li H, Yan XG, Zhou ZW, Yi ZG, He ZX, et al. Alisertib induces cell cycle arrest and autophagy and suppresses epithelial-to-mesenchymal transition involving PI3K/Akt/mTOR and sirtuin 1-mediated signaling pathways in human pancreatic cancer cells. Drug Des Devel Ther. 2015; 9:575–601.
26. Wang X, Lu N, Niu B, Chen X, Xie J, Cheng N. Overexpression of Aurora-A enhances invasion and matrix metalloproteinase-2 expression in esophageal squamous cell carcinoma cells. Mol Cancer Res. 2012; 10:588–96. [PubMed: 22522455]
27. Liu Y, Hawkins OE, Su Y, Vilgelm AE, Sobolik T, Thu YM, et al. Targeting aurora kinases limits tumour growth through DNA damage-mediated senescence and blockade of NF-kappaB impairs this drug-induced senescence. EMBO Mol Med. 2013; 5:149–66. [PubMed: 23180582]
28. Ice RJ, McLaughlin SL, Livengood RH, Culp MV, Eddy ER, Ivanov AV, et al. NEDD9 depletion destabilizes Aurora A kinase and heightens the efficacy of Aurora A inhibitors: implications for treatment of metastatic solid tumors. Cancer research. 2013; 73:3168–80. [PubMed: 23539442]
29. DeRose YS, Gligorich KM, Wang G, Georgelas A, Bowman P, Courdy SJ, et al. Patient-derived models of human breast cancer: protocols for in vitro and in vivo applications in tumor biology and translational medicine. Curr Protoc Pharmacol. 2013; Chapter 14(Unit 14):23. [PubMed: 23456611]
30. Meijering E, Dzyubachyk O, Smal I. Methods for cell and particle tracking. Methods Enzymol. 2012; 504:183–200. [PubMed: 22264535]
31. Kozyreva VK, McLaughlin SL, Livengood RH, Calkins RA, Kelley LC, Rajulapati A, et al. NEDD9 regulates actin dynamics through cortactin deacetylation in an AURKA/HDAC6-dependent manner. Mol Cancer Res. 2014; 12:681–93. [PubMed: 24574519]
32. Kozyulina PY, Loskutov YV, Kozyreva VK, Rajulapati A, Ice RJ, Jones BC, et al. Pro-metastatic NEDD9 regulates individual cell migration via caveolin-1-dependent trafficking of integrins. Mol Cancer Res. 2014
33. Sekulic A, Hudson CC, Homme JL, Yin P, Otterness DM, Karnitz LM, et al. A direct linkage between the phosphoinositide 3-kinase-AKT signaling pathway and the mammalian target of rapamycin in mitogen-stimulated and transformed cells. Cancer Res. 2000; 60:3504–13. [PubMed: 10910062]
34. del Peso L, Gonzalez-Garcia M, Page C, Herrera R, Nunez G. Interleukin-3-induced phosphorylation of BAD through the protein kinase Akt. Science. 1997; 278:687–9. [PubMed: 9381178]
35. Maiuri MC, Le Toumelin G, Criollo A, Rain JC, Gautier F, Juin P, et al. Functional and physical interaction between Bcl-X(L) and a BH3-like domain in Beclin-1. EMBO J. 2007; 26:2527–39. [PubMed: 17446862]
36. Chang F, Steelman LS, Shelton JG, Lee JT, Navolanic PM, Blalock WL, et al. Regulation of cell cycle progression and apoptosis by the Ras/Raf/MEK/ERK pathway (Review). Int J Oncol. 2003; 22:469–80. [PubMed: 12579299]

37. Martelli AM, Tabellini G, Bressanin D, Ognibene A, Goto K, Cocco L, et al. The emerging multiple roles of nuclear Akt. Biochim Biophys Acta. 2012; 1823:2168–78. [PubMed: 22960641]
38. Romanelli A, Clark A, Assayag F, Chateau-Joubert S, Poupon MF, Servely JL, et al. Inhibiting aurora kinases reduces tumor growth and suppresses tumor recurrence after chemotherapy in patient-derived triple-negative breast cancer xenografts. Mol Cancer Ther. 2012; 11:2693–703. [PubMed: 23012245]
39. Zheng XQ, Guo JP, Yang H, Kanai M, He LL, Li YY, et al. Aurora-A is a determinant of tamoxifen sensitivity through phosphorylation of ERalpha in breast cancer. Oncogene. 2013
40. Dar AA, Belkhiri A, Ecsedy J, Zaika A, El-Rifai W. Aurora kinase A inhibition leads to p73-dependent apoptosis in p53-deficient cancer cells. Cancer Res. 2008; 68:8998–9004. [PubMed: 18974145]
41. Fiskus W, Hembruff SL, Rao R, Sharma P, Balusu R, Venkannagari S, et al. Co-treatment with vorinostat synergistically enhances activity of Aurora kinase inhibitor against human breast cancer cells. Breast Cancer Res Treat. 2012; 135:433–44. [PubMed: 22825030]
42. Hiratsuka T, Inomata M, Kono Y, Yokoyama S, Shiraishi N, Kitano S. DHLTauZnNa, a newly synthesized alpha-lipoic acid derivative, induces autophagy in human colorectal cancer cells. Oncol Rep. 2013; 29:2140–6. [PubMed: 23588820]
43. Ren SX, Shen J, Cheng AS, Lu L, Chan RL, Li ZJ, et al. FK-16 derived from the anticancer peptide LL-37 induces caspase-independent apoptosis and autophagic cell death in colon cancer cells. PLoS One. 2013; 8:e63641. [PubMed: 23700428]
44. Zou Z, Yuan Z, Zhang Q, Long Z, Chen J, Tang Z, et al. Aurora kinase A inhibition-induced autophagy triggers drug resistance in breast cancer cells. Autophagy. 2012; 8:1798–810. [PubMed: 23026799]
45. Brockmann M, Poon E, Berry T, Carstensen A, Deubzer HE, Rycak L, et al. Small molecule inhibitors of aurora-a induce proteasomal degradation of N-myc in childhood neuroblastoma. Cancer Cell. 2013; 24:75–89. [PubMed: 23792191]

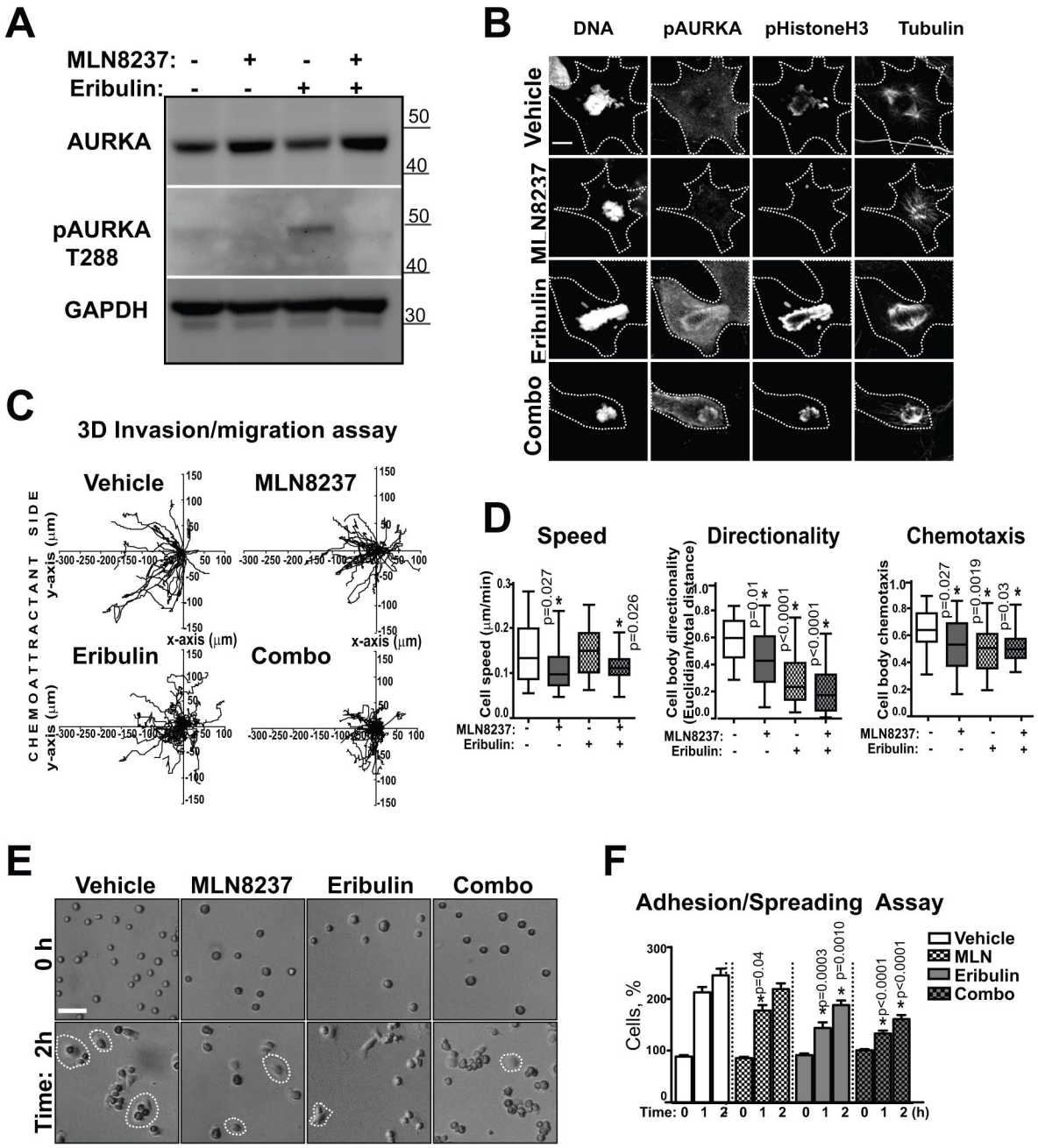


**Figure 1. MLN8237 and eribulin reduce 3D motility/invasion/adhesion of BC cells**

**A** Western blot (WB) analysis of MDA-MB-231LN cells treated as indicated with anti-AURKA total and -pAURKA-T288 antibodies; GAPDH-loading control. **B** Immunofluorescent analysis (IF) of cells as in (A) with anti-pAURKA-T288, -pHistone-H3, -tubulin antibodies and DAPI/DNA, scale bar-10μm. **C** Representative individual MDA-MB-231LN cell tracks, based on bright field time-lapse confocal microscopy images, 0 and 18h in the presence of vehicle/or inhibitors; scale bar-20μm. **D** Quantification of speed, directionality and chemotaxis of moving cells as in (C). Data presented as box and whisker plots of maximum, minimum values from three independent experiments, n=30–50 per

treatment group, ± S.E.M, one-way ANOVA: vehicle vs. treatments. **E** Adhesion and spreading assay. Representative images of MDA-MB-231LN cells treated as indicated, scale bar-20μm. **F** Quantification of cell area based on the images as in (E); cell area normalized to vehicle ±S.E.M, n=100 cells; one-way ANOVA: vehicle vs. treatments.

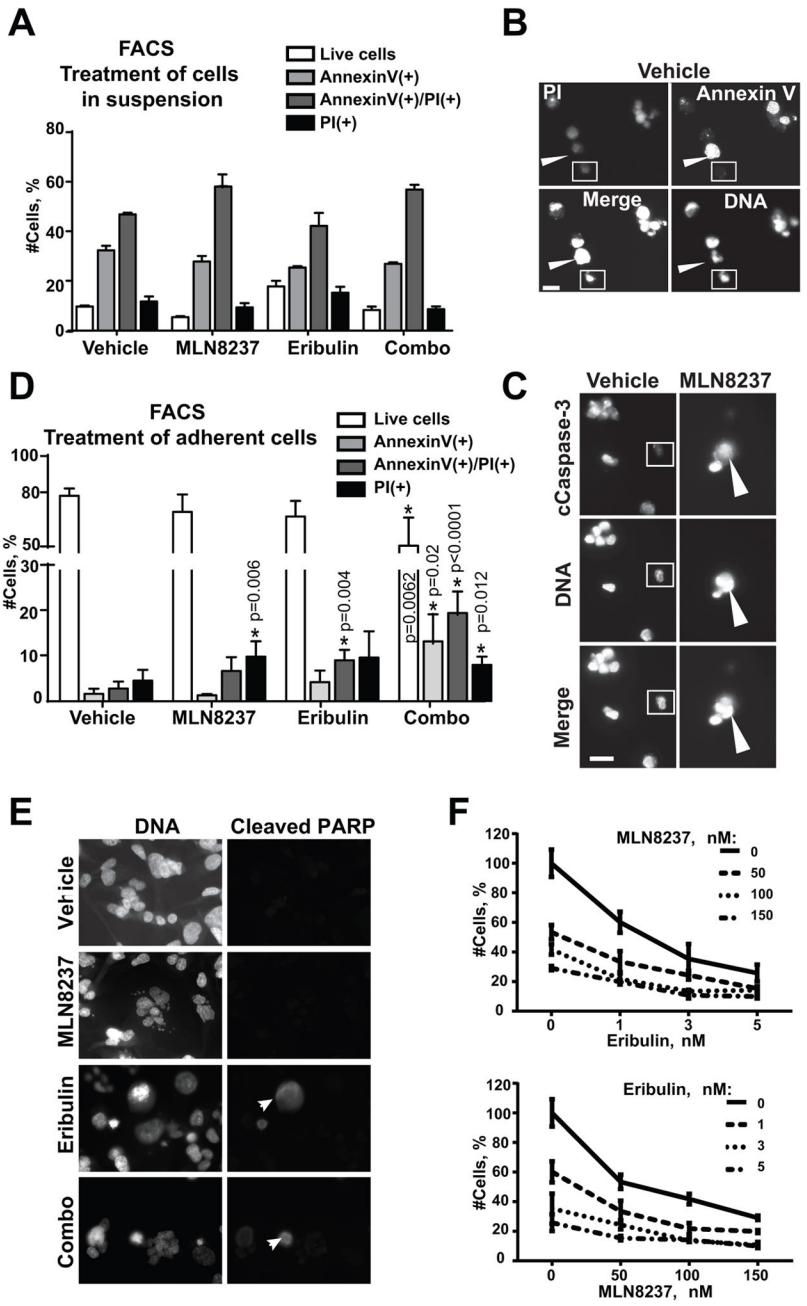


**Figure 2. MLN8237, eribulin, or combination does not affect sensitivity of BC cells to anoikis**

**A** FACS analysis of MDA-MB-231LN cells treated with vehicle/or drugs in suspension for 48h, with Annexin-V, propidium iodine (PI) and Hoechst33342. Graph reperesents % of cells in each category in vehicle/or drug treated groups ± S.E.M, n=3, one-way ANOVA: vehicle vs. treatments. **B** Representative IF images of MDA-MB-231LN cells as in (A) Annexin-V/green, PI/red and DNA/blue; scale bar-20μm; white arrow indicates Annexin-V positive, but PI negative cell; white square indicates Annexin-V and PI negative cell. **C** Representative IF images of MDA-MB-231LN cells as in (A) with anti-cleaved-caspase-3 antibodies/red, DNA/blue; scale bar-20μm; white arrow indicates cleaved-caspase-3 positive

cell; white square indicates caspase negative cell. **D** FACS analysis of attached cells treated with vehicle/or drugs and stained as in (A). All cells including those found in suspension were collected and analyzed. % of cells ± S.E.M, n=3, one-way ANOVA: vehicle vs. treatments. **E** Representative IF images of MDA-MB-231LN cells as in (D) with anti-cleaved-PARP/green antibodies DNA/blue; scale bar-20μm; white arrows indicate apoptotic cells. **F** Cell proliferation/death analysis of MDA-MB-231LN cells treated with serial dilutions of MLN8237 and eribulin as indicated for 48h. The % of live/dead cells was calculated using trypan blue staining.

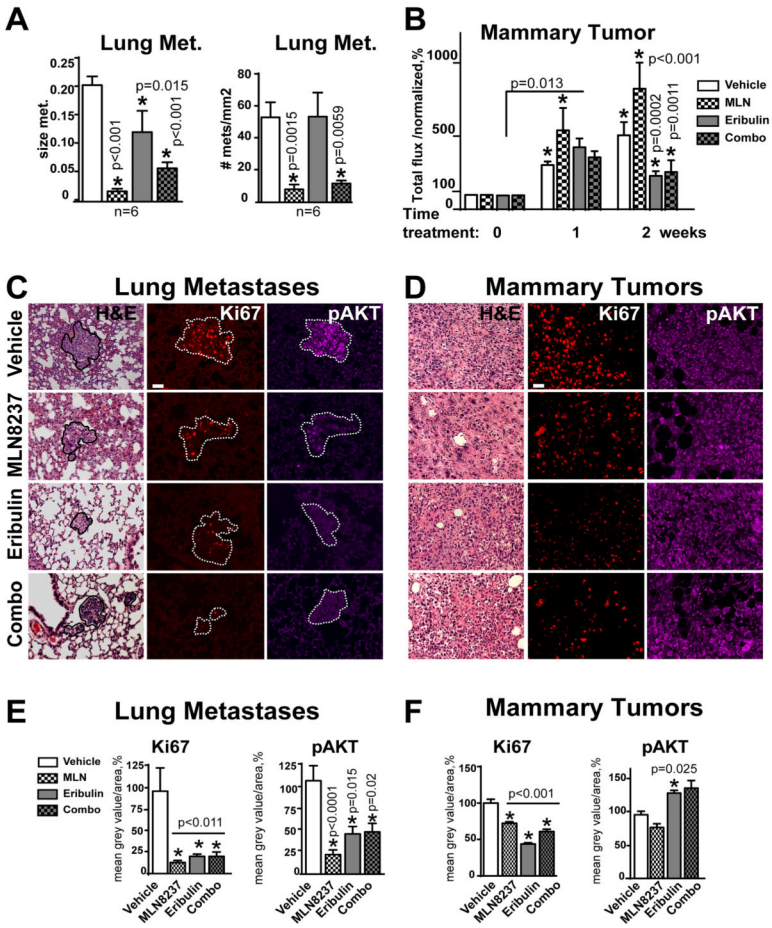


**Figure 3. MLN8237 and MLN8237/eribulin combination reduces metastases *in vivo***

**A** Quantification of size and number of pulmonary metastases as in (C). **B** Quantification of mammary tumor growth in MDA-MB-231LN-xenografts based on bioluminescence imaging (average radiance, p/s/cm$^2$/sr) normalized to initial tumor volume (before drug application) at time point zero, referenced as 100%; one-way ANOVA: vehicle vs. treatments at each time point. **C–D** Representative images of H&E and F-IHC staining of pulmonary tissue (metastases defined by the white outline based on H&E), or **D** Mammary MDA-MB-231LN-xenograft tumor with anti-Ki67/red, -pAKT/purple antibodies. Scale bar - 30μm **E–F** Quantification of F-IHC as in (C–D); multiple metastases/or tumors; 5–6 animals, n=3; % to control; one-way ANOVA: vehicle vs. treatments;

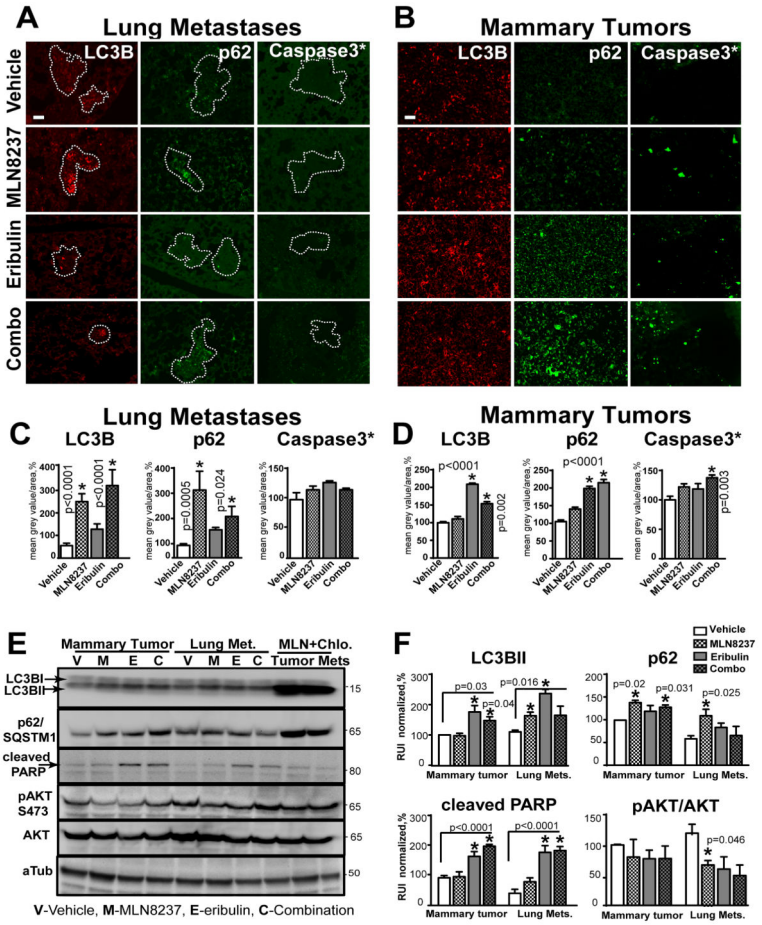


**Figure 4. MLN8237/eribulin combination induce cytotoxic autophagy and apoptosis**

**A–B** Representative images of F-IHC staining of pulmonary tissue (**A**-metastases defined by the white outline) or **B** mammary MDA-MB-231LN-xenograft tumor with -LC3B/red, -SQSTM1/p62/green, -cleaved-caspase-3*/green antibodies. Scale bar - 30μm **C–D** Quantification of F-IHC as in (A–B); multiple metastases/or tumors; 5–6 animals, n=3; % to control; one-way ANOVA: vehicle vs. treatments. **E** WB analysis of LC3B, p62, cleaved PARP, pAKT, AKT, alpha-tubulin (loading control) with respective antibodies in MDA-MB-231LN cells isolated from vehicle-treated mice, expanded *in vitro* and treated with drugs for 48h as indicated; last two lanes contain lysates treated with MLN8237+chloroquine (Chlo.). **F** Quantification of digital images as in (C) using GeneTools software, mean grey value of corresponding band/area (% of vehicle, normalized to tubulin) ±S.E.M, n=3, one-way ANOVA: vehicle vs. treatments.

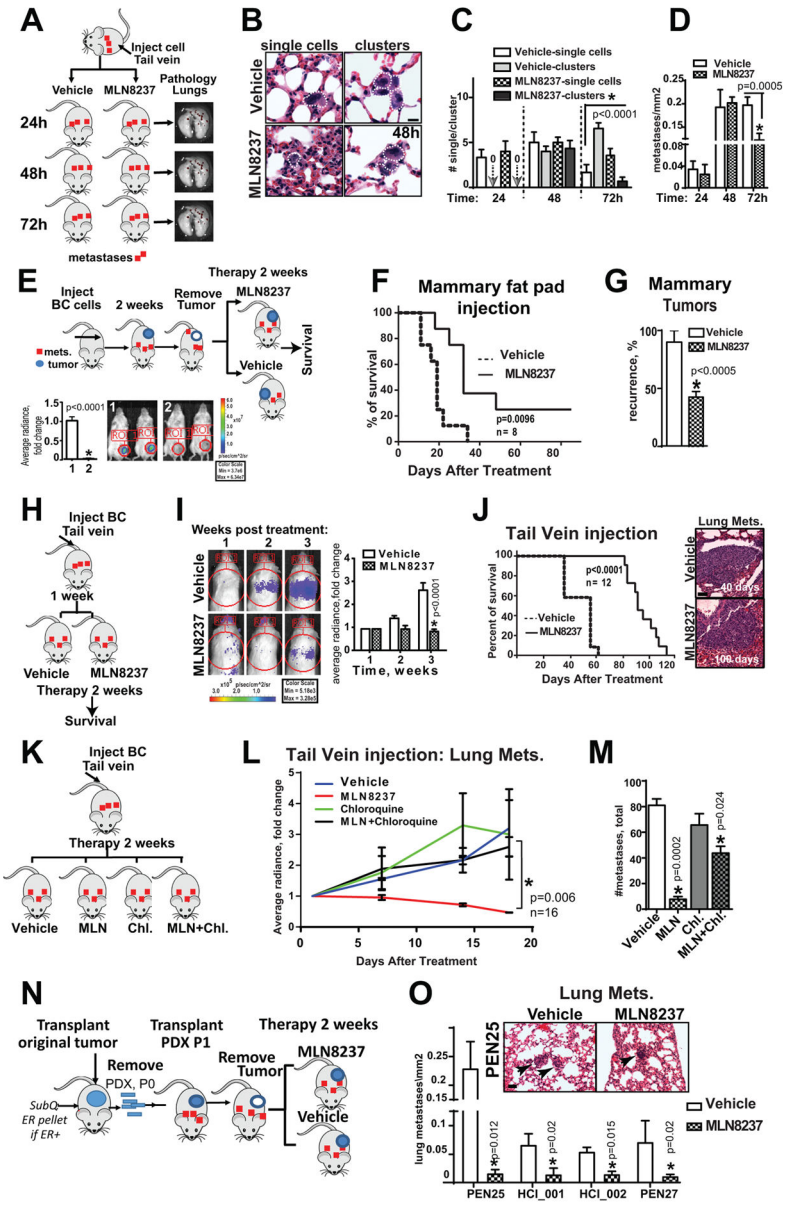


**Figure 5. MLN8237 reduces metastatic colonization and improves overall survival**

**A** Experimental design to test impact of MLN8237 on metastatic colonization. **B** Representative H&E images of lung tissue (48h), white line outline tumor cell/s, scale bar-10μm. **C** Quantification of single cell/clusters metastases as in (B) 24–72 hours, two mice/time point, three independent experiments, one-way ANOVA: vehicle/MLN8237. **D** Quantification of total number of metastases as in (A–B), one-way ANOVA, vehicle/MLN8237. **E** Experimental design to test impact of MLN8237 on overall survival in orthotopic models. Representative BLI images of mice before and after the surgery. Average radiance/ROI, fold of change; all animals in this study died from pulmonary metastatic outgrowth. No difference in BLI/or pathology was documented at the point of euthanasia. **F** Kaplan-Meier survival curves, mice as in (E) treated in adjuvant setting, 8 mice/group, n=2. **G** Percent of animals as in (E) with recurrent tumors, identified during necropsy; paired t-

test. **H** Experimental design to test the impact of MLN8237 on overall survival in tail vein model of systemic disease spread. **I** Representative BLI images of mice 1–3 weeks post injection; Quantification of average radiance, fold of change (graph, right); one-way ANOVA. *Imaging at later time points was not possible due to respiratory distress-caused death in vehicle group*. **J** Kaplan-Maier survival curves, mice as in (H) treated with vehicle or MLN8237, 12 mice/group, two independent experiments; representative H&E images of metastases at the end point. **K** Experimental design to test the impact of MLN8237 in combination with chloroquine on metastatic colonization. **L** Quantification of average radiance/lungs, fold of change; treatment as indicated for 2 weeks, n=16, one-way ANOVA. **M** Quantification of metastases at the end point/mm2, n=6 lungs/group, one-way ANOVA. **N** Experimental design to test the impact of MLN8237 on lung metastases in orthotopic model using PDXs. **O** Quantification of total number of metastases as in (K) immediately after 2 weeks of treatment, multiple t-tests, Holm-Sidak method, vehicle/MLN8237; representative H&E images of metastases at the end point, black arrows indicate lung metastasis.

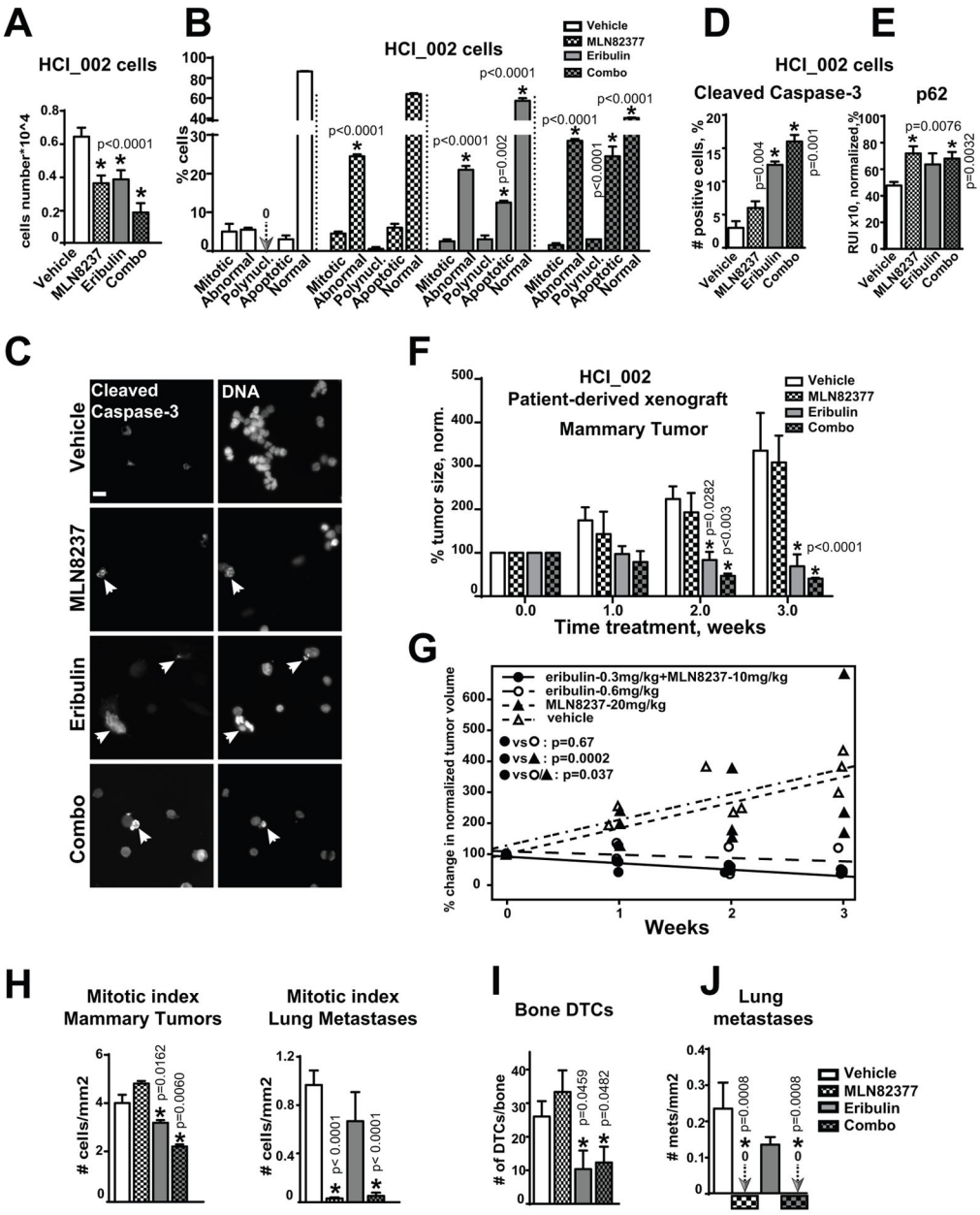


**Figure 6. MLN8237+eribulin reduces primary tumor, metastases and dissemination of cancer in patient-derived xenograft models**

**A** HCI_002 cell growth analysis, 48h; vehicle, 100nM-MLN8237, 3nM-eribulin, or combination; n=3, one-way ANOVA: vehicle vs. treatments. **B** Analysis of the nuclear morphology, cells as in (A); one-way ANOVA: vehicle vs. treatments in each category: mitotic, abnormal nucleus, polynucleated, apoptotic, normal. **C** Representative IF images of HCI_002 cells treated as in (A) with anti-cleaved-caspase-3/green antibodies, DNA, scale bar-20μm; white arrow identifies apoptotic DNA. **D** Quantification of cleaved-caspase-3 positive cells using IF images as in (C); one-way-ANOVA: vehicle vs. treatments. **E** IF-based analysis of cells as in (A) with p62 antibodies; the relative intensity (RIU) of the IF signal from 3 independent experiments; 100 cells/treatment, one-way-ANOVA: vehicle vs.

treatments. **F** Tumor volume analysis of HCI_002-PDX mammary xenografts in three cohorts, n=6/cohort; Tumor growth was normalized to time point zero of treatment (100%) in each cohort; one-way ANOVA: vehicle vs. treatments. **G** Statistical analysis of the data as in F using mixed model; **H** Mitotic index analysis of metastases/lungs or mammary tumors as in (F), n=50 cells/treatment in 3 experiments, t-test. **I** Analysis of disseminated tumor cells in femurs of mice as in (F); n=2/mouse; one-way ANOVA: vehicle vs. treatments. **J** Quantification of lung metastases; serial sections of lungs from three mice/treatment, one-way ANOVA: vehicle vs. treatments. MLN8237 and combination treated mice did not have metastases; arrows and zero signs visualize the absence of signal.

**Table 1**

The analysis of drug interaction in cell growth assay as in Fig. 2F using multiple statistical methods described in Supplementary Methods.

| Models | Drug interaction Parameter | | | Estimated | 95% CI | Conclusion |
|---|---|---|---|---|---|---|
| | Syn. | Add. | Ant. | | | |
| | *II* < 1 | *II* = 1 | *II* > 1 | | | |
| Chou and Talalay | Eribulin=1, MLN =50 | | | 0.688 | (0.573, 0.825) | Synergy |
| | Eribulin=3, MLN =100 | | | 0.468 | (0.334, 0.654) | Synergy |
| | Eribulin=5, MLN =100 | | | 0.669 | (0.519, 0.866) | Synergy |
| | Eribulin=3, MLN =150 | | | 0.427 | (0.269, 0.677) | Synergy |
| | Eribulin=5, MLN =150 | | | 0.505 | (0.345, 0.738) | Synergy |
| Greco | α>0 | α=0 | α<0 | 0.949 | (0.187, 1.711) | Synergy |
| Machado | 0<h<1 | h=0 | h>1 | 0.613 | (0.474, 0.753) | Synergy |

**Table 2**

Analysis of drug interactions using Chou Talalay method.
Analysis Chou and Talalay Syn II < 1, Add II = 1, Ant II > 1

| Drugs/nm | Estimated | 95%, CI | Conclusion: |
|---|---|---|---|
| Eribulin=1, MLN =50 | 0.538 | (0.334, 0.741) | Synergy |
| Eribulin=3, MLN =100 | 0.481 | (0.329, 0.641) | Synergy |
| Eribulin=5, MLN =100 | 0.645 | (0.501, 0.852) | Synergy |
| Eribulin=3, MLN =150 | 0.341 | (0.247, 0.777) | Synergy |